http://dx.doi.org/10.5012/bkcs.2011.32.11.4027

A Novel Approach to Controlling $CaCO_3$ Crystalline Assembly by Changing the Concentration of Poly(aspartic acid)

Hongjian Zhou, Yanmin Gao,‡ Sungu Hwang, Dongyun Lee,† Jung Youn Park,§ and Jaebeom Lee*

*Department of Nanomedical Engineering, †Department of Nanofusion Engineering, College of Nanoscience and Nanotechnology, Pusan National University, Miryang 627-706, Korea. *E-mail: jaebeom@pusan.ac.kr*
‡School of Material Science and Engineering, Jiangsu University of Science and Technology, Zhenjiang 212003, People's Republic of China. §Department of Biotechnology Research, National Fisheries Research and Development Institute, Busan 619-705, Korea
Received August 23, 2011, Accepted September 20, 2011

$CaCO_3$ crystalline structures having novel assemblies were *in situ* fabricated as analogs of naturally occurring proteins and polysaccharides for biomineralization. The calcite crystal was mineralized in a poly(vinyl alcohol)-Ca^{2+} complex film immersed in a Na_2CO_3 solution containing poly(aspartic acid). The morphology and size of the $CaCO_3$ crystals were tuned by varying the concentration of poly(aspartic acid). The mechanisms of their nucleation orientation and formation were investigated experimentally and through molecular dynamics (MD) simulations in order to obtain a better understanding of the interactions between the polymers and the crystal at the molecular level. Both the MD results and experimental results indicate that the interaction between PVA and calcite mainly depends on the concentration of the polymer. The novel approach proposed herein for the fabrication of inorganic crystalline assembly structures can be used to fabricate precise crystalline structures.

Key Words : Molecular dynamics simulation, Biomineralization, Crystalline assembly structures

Introduction

Biomineralization is the process by which living organisms secrete inorganic minerals in the form of highly ordered and complex structures such as skeletons, shells, teeth, etc..[1-7] A remarkable feature of naturally occurring materials – for example, the porous silica exoskeleton observed in diatoms and natural honeycombs – is their highly ordered structures and finely carved appearance. Such highly ordered structures with sizes ranging from nanometers to millimeters are characteristic of biological structures, introducing the capability to meet the physical or chemical demand occurring at these different levels.[8] Such complex and highly ordered structures of natural materials have inspired materials scientists to develop new types of high-performance engineering materials.

By adopting the biomineralization-inspired assembly, many inorganic particles with controllable morphology have been prepared *in vitro* by using natural and synthetic polymers.[9-21] Owing to the remarkable progress in the research on biomimetic mineralization, the mechanisms underlying the formation of biominerals have been established, on the basis of which a number of novel designs and high-performance structures have been developed.[22,23] Much effort has been focused on exploring the interaction between additives and certain crystal faces and the relationship between primary and secondary structures of organic additives and crystal morphology.[24,25] Recently, a series of quantitative analyses on the formation of prenucleation clusters during the early stages of $CaCO_3$ precipitation in the absence and presence of such additives have been carried out, and it has been found that short-range ordering occurs much before the formation of the prenucleation clusters.[26,27] Therefore, it is necessary to investigate whether the final morphology and polymorphs of a crystal are affected by the ordering of its structure during the formation of prenucleation clusters or by the addition of additives to different mineral phases. Moreover, to the best of our knowledge, there have been few studies on macroscopic $CaCO_3$ materials with complicated substructures and sizes ranging from the nanoscale to the microscale.[28-30]

In this study, we investigate the assembly behavior of $CaCO_3$ crystals with sizes ranging from the nanoscale to the microscale on a poly(vinyl alcohol) (PVA) film; the growth of the crystals on the film is carried out by changing the concentration of poly(aspartic acid) (pAsp), the crystal modifier. We focused on specific, coordinated interactions between the surfaces of the polymers and minerals by using pAsp and PVA as the analogs of naturally occurring biominerals of modifier (acid-soluble proteins) and substrate (polysaccharides). The co-effect of pAsp and PVA on the synthesis of the $CaCO_3$/polymer membrane was systematically characterized. Molecular dynamics (MD) simulations were also carried out in order to obtain a better understanding of the interactions between the polymers and the crystal at the molecular level.

Experimental Method

Materials. We purchased pAsp (M_w: about 5000) from

Shandong Li Bang Fine Chemicals Company Limited (Jinan, China) and obtained PVA (M_w: about 125000) from Sinopharm Chemical Reagent Company Limited (Shanghai, China). $CaCl_2$ and Na_2CO_3 were of the analytical-reagent grade. Deionized water (over 18 MΩ) was used throughout the experimental procedure.

Preparation of $CaCO_3$ Particles. The salt solution contained 0.1 M $CaCl_2$ and 0.1 M Na_2CO_3 as source ions for $CaCO_3$. Various concentrations of PASP were prepared as a modifier of crystallization in the salt solution. pH of the solution was regulated at 7.5. Experiments were maintained in a closed glass beaker for seven days at 25 °C. The final particles were rinsed with deionized water and dried for characterization.

Preparation of the PVA Film and $CaCO_3$ Films. Ten grams of PVA was dissolved in 100 mL of deionized water at 100 °C, and 1.11 g of $CaCl_2$ was dissolved in the aqueous PVA solution. Solid PVA films were coated on a glass substrate by dip coating. The films, after being dried at 25 °C, were washed with deionized water. For the preparation of $CaCO_3$ films, pAsp was dissolved in an aqueous Na_2CO_3 solution at two different concentrations (10 mg/mL and 20 mg/mL). The PVA-coated glass substrate was immersed in a Na_2CO_3 solution containing various concentrations of pAsp. The substrate obtained after a reaction period of seven days at 25 °C was rinsed with deionized water and dried for characterization.

Molecular Dynamics (MD) Simulations. MD simulation was conducted by using Material Studio (MS) v4.2 package (Accelrys, San Diego, CA) and the condensed-phase optimized molecular potentials for atomistic simulation studies (COMPASS) force field. The COMPASS force field is a general all-atom force field for atom simulation developed using state-of-the-art *ab initio* and empirical parameterization techniques; it is applicable to both organic and inorganic materials.[31] Validation studies of the COMPASS force field have demonstrated its ability to accurately predict the structural, chemical, and physical properties of a broad range of molecules and condensed phases.[31] The process of constructing the proposed model is explained in detail in the Supporting Information section.

Characterization. A scanning electron microscope (SEM, JEOL-6480) was used for observing the morphologies of the products. The samples were carefully mounted on copper stubs with a double-sided carbon tape and then coated with a thin layer of gold before examination. X-ray diffraction (XRD, D/max2500VB3) was performed with Cu Kα radiation (λ = 1.5148) *via* a rotating anode at 40 kV and 200 mA. The data were collected in steps of 0.05°/10 s, with the diffraction angle (2θ) ranging from 10° to 90°.

Results and Discussion

Synthesis of the $CaCO_3$/Polymer Membrane. After the synthesis of $CaCO_3$ on the PVA membrane, the membranes were directly observed using SEM and XRD. In the absence of pAsp, we obtained precipitated crystals that were regular, rhombohedral calcite particles (Figure 1(a)). As shown in Figure 1(a), many of the particles had cleavage faces of (104) orientation, which is a well-known crystallographic orientation in calcite and also the most thermodynamically stable face.[32-34] From the XRD result, however, diffraction peaks of the vaterite phase (ICSD card no: 33-0268) appeared following addition of 5 mg/mL PASP, and diffraction intensity of the calcite phase decreased, as shown in Figure 2(b). Along with the increase in PASP concentration, the gradual disappearance of diffraction peaks of calcite, along with a gradual increase of vaterite, can be seen in Figure 2(c). As shown in Figure 2(d), the typical vaterite phase was eventually confirmed following addition of 20 mg/mL PASP. The above results indicate an important role for PASP in control of crystal polymorphs in homogeneous nucleation. PASP is sufficient for control of transformation between calcite and vaterite in solution. In Figure 2(b), we confirmed that the strongest diffraction peak is indexed as a typical (104) plane of calcite with the strong diffraction peak indexed as PVA. With the addition of pAsp, other crystallographic orientations were observed; these are explained in detail later in this section.

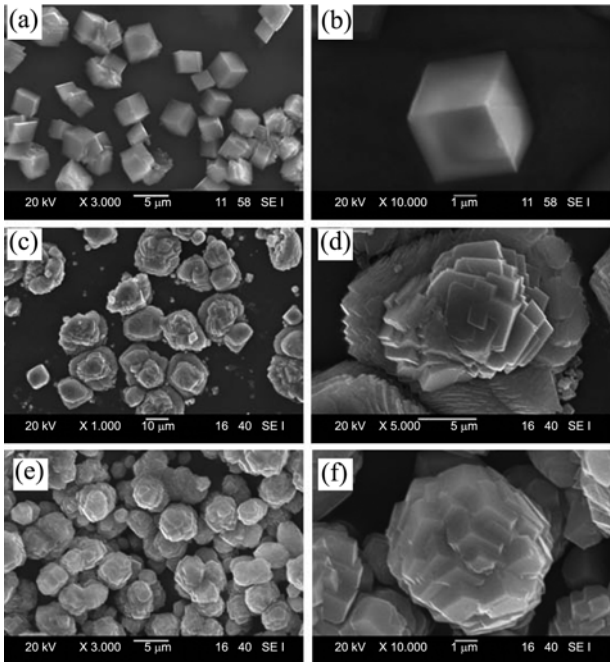

Figure 1. SEM morphologies of the calcite crystals grown on PVA membranes: (a) and (b) without additives, regular rhombohedral shape; (c) and (d) after the addition of 10 mg/mL pAsp, flower-like crystals; (e) and (f) after the addition of 20 mg/mL pAsp, pineapple-like crystals.

The predominant crystallographic orientations of the calcite crystals were quantitatively analyzed from the XRD spectra.[35,36] For a quantitative analysis of the orientational uniformity of the crystals (Table 1), we normalized the measured intensities of the peaks in these spectra by the standard intensities of the peaks corresponding to randomly oriented calcite powder, the values of which were obtained from the ICSD standard data. Note that we used the most

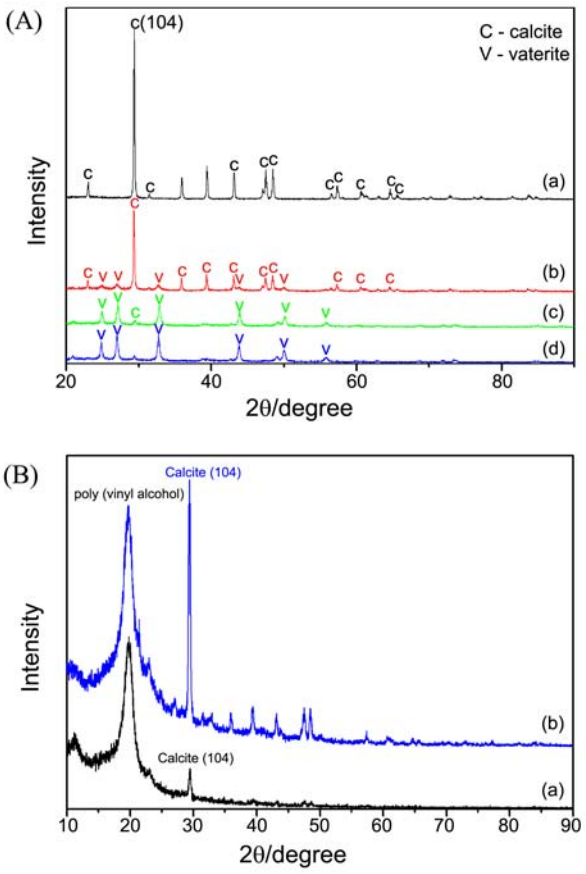

Figure 2. (A) XRD patterns of $CaCO_3$ deposition produced at various concentrations of PASP. (a) without additives; (b) after addition of 5 mg/mL PASP; (c) after addition of 10 mg/mL PASP (d) after addition of 20 mg/mL PASP. (B) XRD patterns of $CaCO_3$/PVA membrane: (a) without additives and (b) after the addition of 20 mg/mL pAsp.

distinguishable peaks, indicated as "c", to calculate the predominant crystallographic orientations. The percentage of calcite crystals in different orientations (*hkl*) was estimated using the following equation:

$$\%\text{hkl} = 100 \times \frac{I_{hkl}/I^*_{hkl}}{\Sigma_{hkl}(I_{hkl}/I^*_{hkl})}, \quad (1)$$

where I_{hkl} is the intensity of peaks obtained from the ICSD standard data (card no.: 05-0586) shown in the XRD profile for randomly oriented calcite powder and I^*_{hkl} is the measured intensity of the peaks from the XRD profiles of calcite crystals grown on different surfaces.

The results show that the crystals grown on the PVA membrane have a pronounced orientational uniformity: the predominant nucleating planes were (104) for PVA [70.8% for the (104) reflection] and (104) for PVA/pAsp [25.3% for the (104) reflection]. From this result, we can see that 70.8% of the crystal faces of calcite have the orientation of the (104) plane. However, upon adding pAsp, the percentage of crystal faces with the orientation of the (104) plane decreased. As shown in Figure 1(f), the addition of pAsp promotes the formation of calcite with pineapple-like morphology that includes some other orientations; however, the (104) planes are still predominant in the pineapple-like morphology.

Table 1. Crystallographic orientation of the calcite crystals grown on the PVA membrane; the results were obtained from the XRD data

hkl	Standard int, I^{*a}	PVA		PVA/pAsp	
		I^b	%^{c}	I^b	%^{c}
104	100	100	**70.8**	100	**25.3**
110	14			7.9	14.3
113	18			9	12.7
202	18			6	8.4
018	17	7	29.2	10	14.9
116	17			10	14.9
122	8			3	9.5

[a]ICSD (card no.: 05-0586) data showing the intensities of peaks in the XRD profile for randomly oriented calcite powder. [b]Measured intensity of peaks in the XRD profiles of calcite crystals grown on different surfaces. [c]Percentage of crystals in different orientations estimated using Equation 1.

Weiner *et al.* discovered that the antiparallel β-pleated sheet found in the matrix of mollusk shells contains Asp-X-Asp structures (where X is a neutral residue).[3;37] These periodic structures may bind Ca^{2+} ions to form the (001) faces of calcite or aragonite crystals.[38-40] Hou *et al.*[3] found that the EDTA-insoluble protein membranes extracted from the nacreous layer of mollusk shells (*M. edulis*) promote nucleation through structural matching with the (001) faces of calcite. Our observations suggest a similar structural correspondence between the PVA membrane and the fabricated calcite crystals (Figures 1(a) and 1(b)). The lattice parameters of synthetic calcite calculated from the XRD patterns were found to be as follows: a = 4.988 Å and c = 17.08 Å; these values are in good agreement with the literature values for rhombohedral symmetry (in hexagonal axes): a = 4.991 Å and c = 17.061 Å.[32] The interplanar angle between the (001) and (104) planes calculated by using a general equation[36] based on the experimental data was found to be approximately 44.61°. By using this value, we performed crystallographic analysis of the fabricated calcite crystals by following a previously reported method.[32,33] Further, (104)-oriented twin crystals inclined at 44.62° relative to the [001] direction and perpendicular to the (001) plane were grown. On the basis of these results, we suggest the following mechanism for the formation of calcite. Figure 3 shows the schematic representation of the process of crystal formation. Nucleation takes place at point O and grows in the [001] direction, perpendicular to the membrane surface. Calcite crystals nucleate in the inductive region of the PVA membrane. These nuclei have the same [001] directions, as shown in Figure 3. By referring to the matching model, it can be inferred that their [100] or [010] directions may be the same or may differ by an angle of 60°, since calcite belongs to a hexagonal system.[3] Similarly, the prismatic layers in mollusk shells are (001)-oriented calcite crystals.[41] Therefore, the results indicate that the coordinated interactions between the hydroxyl groups in a natural, insoluble

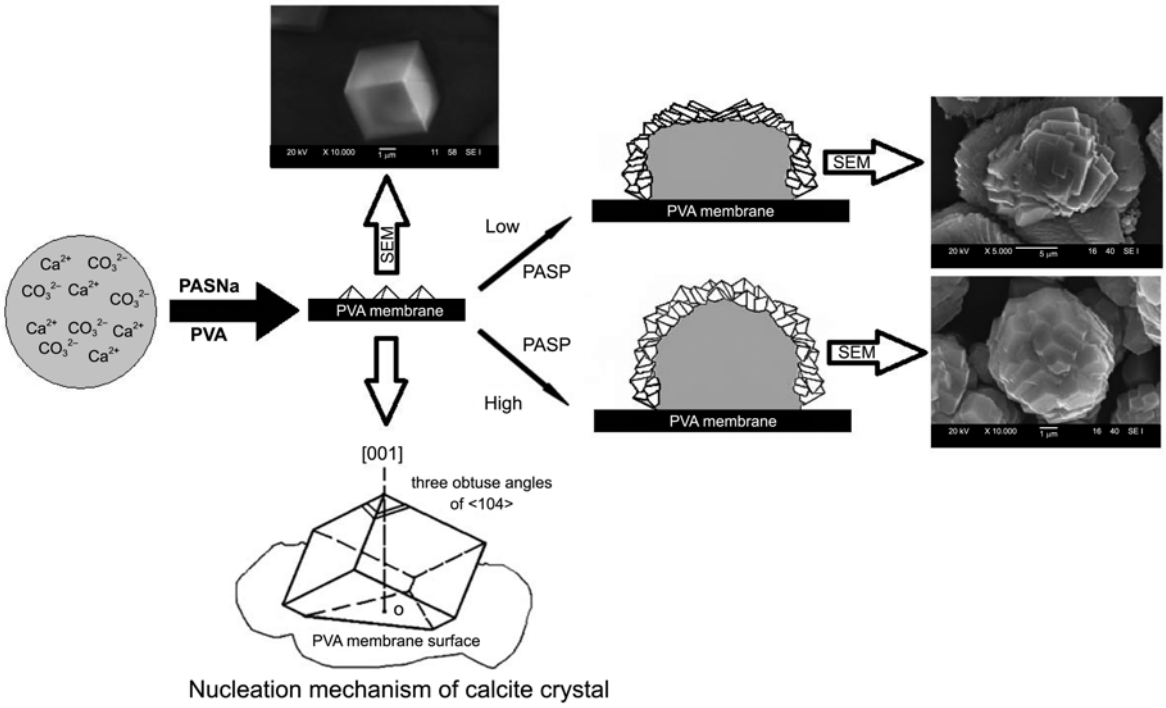

Figure 3. Schematic illustration of crystal growth on the PVA film; the growth of the crystals on the film is carried out by changing the concentration of pAsp.

matrix may play a significant role in biomineralization.

Meanwhile, flower-like crystals are formed in the presence of pAsp; some crystal particles have an agglomerated appearance (Figures 1(c) and 1(d)), which is caused by polynuclear growth. The nuclei are agglutinated by surface-adsorbed pAsp molecules and grow together as a single particle. Therefore, under a higher concentration of pAsp, the agglomerated appearance becomes more elaborate. In Figures 1(e) and 1(f), the aggregated orbicular particles are composed of a number of little, pineapple-like pyramids of calcite. As in the case of the axes of the three planes discussed earlier, all the [001] directions appeared capable of extension toward the center of the sphere-like particle.[42] In macro-observation, this means that the arrangement of all obtuse-triangular pyramids in the sphere-like particle will either be identical or mirror-symmetric (Figure 1(f)). The formation model of the aggregated orbicular particles is shown in Figure 3.

Undoubtedly, the results obtained indicate the adsorption of the selected polypeptides on the calcite surface. Interactions between pAsp and the calcite surface occur as a result of the formation of coordinative bonds between the Ca^{2+} ions at the surface and the side-chain carboxylic groups of the polypeptide.[14] The adsorption of the pAsp molecules on the calcite surface is a result of the electronegativity of the carboxyl groups ($-COO^-$). The stereochemical structure of the polypeptide is similar to that of the $C-O_3$ triangle in the calcite crystal lattice, and the COO^- groups of pAsp may especially bind the surface Ca^{2+} ions, thereby controlling the growth of the calcite crystal.[43] Similarly, these results indicate that the coordinated interactions between the carboxylic groups of the natural, soluble glycoproteins found in aspartic acid residues, which are extracted from the calcitic layers of mollusk shells, may play a significant role in biomineralization. Addadi *et al.*[44] reported that in the adsorbed state, poly-L-aspartic acid assumed a β-sheet structure and random coil conformation. The predicted secondary structure of pAsp in an aqueous solution suggests that pAsp accounts for almost 50% of the β structures (β-strand and β-turn). When adsorbed on the surface of a solution containing Ca^{2+} ions, pAsp tends to adopt extended regions in β-pleated sheet conformation. The extended conformation assumed by the polypeptide in the β-sheet region favors the formation of coordinate bonds between its side-chain carboxylate groups and Ca^{2+} ions at the calcite surface.

With reference to the polymorph formation described herein, the proposed model of strong coordinated interactions between pAsp and the calcite surface is consistent and complementary to the mechanism of functioning of the Asprich proteins isolated from the calcite layer of mollusk shells. We keep in mind that not only the stereochemistry but also other parameters such as the sequence and structure of the polypeptide, accompanied by specific microenvironments, including ionotropy, charge, and the presence of specific insoluble macromolecules, can play a decisive role in the formation of a particular polymorph.[14,41,43-47]

We believe that these results might enable us to understand the process of biomineralization. A good understanding of the process of biomineralization delivers new tools and possibilities into the hands of chemists for the generation of crystalline nano- and mesostructures in a much broader and potentially useful way. However, there is still

much to be learned about the forces guiding crystal assembly and the exact formation mechanisms.

Molecular Dynamics (MD) Simulation. The use of MD simulation is an effective method for the study of the interactions between nanoparticles, polymers, and small molecules. The MD simulation technique is based on the force field of atoms that can simulate the properties of a system, with a calculated space length ranging from several angstroms to several nanometers. Therefore, in order to get an insight about the assembly mechanisms of the $CaCO_3$ crystal under the action of a polymer at the molecular level, we designed three models on the basis of our experimental results: (i) calcite (001)/PVA model, (ii) calcite (104)/pAsp-low (low concentration) model, and (iii) calcite (104)/pAsp-high (high concentration) model. The calcite (001)/PVA model simulated the nucleation of calcite crystals on the PVA membrane; the calcite (104)/pAsp-low model and the calcite (104)/pAsp-high model simulated calcite crystals assembly under the action of pAsp with low and high concentration, respectively.

Calcite/Polymer Interaction. Computation of the interaction energy between a polymer and calcite is important to understand the physisorption of calcite with the polymer. We built the PVA model and the pAsp model with the calcite (001) and (104) planes using Material Studio (MS) v4.2 package (Accelrys, San Diego, CA) (See Figs. S1, S2, and S3 in the Supporting Information section).

A single-layer slab structure with a periodic boundary condition was used to build the model of the PVA membrane with the calcite (001) plane and the model of the pAsp molecule with the calcite (104) plane (Figure 4). The application of periodic boundary conditions enables us to investigate the adsorption behavior of calcite with a desired coverage on an infinite PVA surface and the calcite crystal surface. In the calcite/PVA model, there are two layers of PVA molecules: one fixed and the other movable. The former is analogous to the upper surface of the PVA membrane, and the latter is analogous to the surface in contact with the calcite surface. A 5000-step energy minimization was performed at the initial stage of the layer-model construction. MD simulations were conducted on the two models under the NVT ensemble with a time step of 1 fs for 1500 ps until the system reached equilibrium. Subsequently, additional 100-ps MD simulations were conducted for analysis. Snapshots of the calcite/PVA model, calcite/pAsp-low model, and calcite/pAsp-high model before and after the MD simulations are shown in Figure 4. The binding energies, nonbonding energies, and mean-squared displacements of these three models were calculated after conducting the MD simulations.

Interaction between Calcite and the Polymers. The interaction between calcite and the polymers can be evaluated on the basis of the binding energy between the crystallographic surfaces in calcite and the polymer molecules. Table 1 shows the binding energies between the polymer chains and the calcite surface; these were calculated from the following equation:

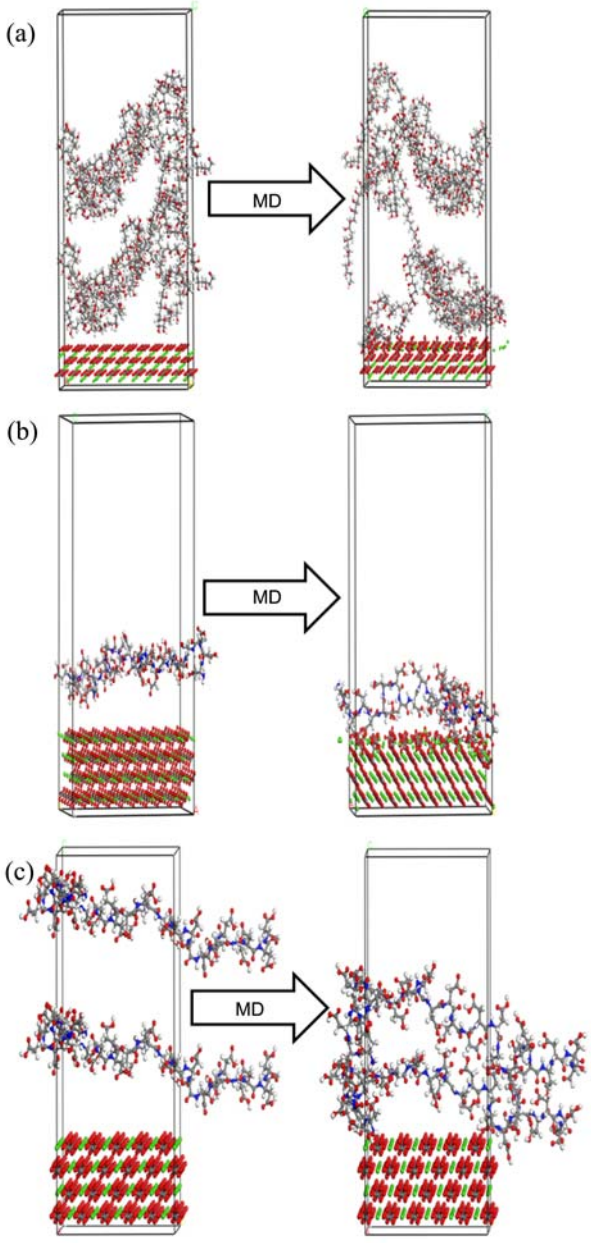

Figure 4. Snapshots of (A) the calcite/PVA model, (B) the calcite/pAsp-low model, and (C) the calcite/pAsp-high model before (left) and after (right) MD simulation.

$$E_{binding} = E_{calcite} + E_{polymer} - E_{calcite+polymer}, \quad (2)$$

where $E_{calcite}$ is the energy of the calcite surface, $E_{polymer}$ is the energy of the polymer chains, and $E_{calcite+polymer}$ is the energy of the calcite surface with the polymer. Note that a high binding energy indicates high adhesive strength between the polymer and the calcite surface.[48,49] The binding energies between calcite and the polymer were calculated from the COMPASS force field, the results of which are listed in Table 2.

As already mentioned in the Results and Discussion section, the calcite crystals nucleate in the inductive region of the PVA membranes through interfacial matching to the

Table 2. Binding energies between calcite and the polymers

Surface	Polymer	$E_{calcite+polymer}$ (kJ·mol^{-1})	$E_{polymer}$ (kJ·mol^{-1})	$E_{calcite}$ (kJ·mol^{-1})	E_{bind} (kJ·mol^{-1})
(001)	PVA	198073.63	−8519.85	214507.68	7914.20
(104)	pAsp-low	−594887.02	−4289.06	−590536.49	61.47
(104)	pAsp-high	−555080.53	−7711.54	−547127.61	241.38

(001) faces. By simply varying the concentration of pAsp added to calcite, the calcite crystal was assembled to form flower-like and pineapple-like particles. Therefore, the calcite/PVA model was built for the simulation of the nucleation of the calcite crystals in the PVA membranes; the calcite/pAsp-low (B) and calcite/pAsp-high (C) models were built for the simulation of the assembly of the calcite crystals under the action of pAsp with low and high concentration, respectively. As shown in Table 2, the results clearly indicate that the polymer was adsorbed on the crystal surface because the binding energies of the different systems were positive. It is more important to ensure that the binding energy between calcite and PVA is sufficiently strong to induce nucleation of the calcite (001) face. Moreover, the binding energy of the calcite/pAsp-high model is four time higher than that of the calcite/pAsp-low model. This implies that the assembling force of the calcite crystals under the action of high-concentration pAsp is different from that of the calcite crystals under the action of low-concentration pAsp. As shown in the SEM images (Figures 1(d) and 1(f)), the calcite crystal unit cells comprised flower-like and pineapple-like particles, but the elaborate degree of assembly was different between the two kinds of particles because of the different assembling forces of high- and low-concentration pAsp. Therefore, the simulation results are consistent with the experimental results, both of which provide abundant proof that a variation in the concentration of pAsp played a significant role in the assembly of the calcite crystal.

The non-binding energies between the calcite particles and the polymers were calculated from the COMPASS force field, the results of which are listed in Table 3. The negative and positive values of interaction energy correspond to the attractive and repulsive forces between calcite and the polymer, respectively. By comparing the non-bonding energies between calcite and the three polymers, it can be clearly inferred that the interaction between PVA and calcite mainly depended on the Coulomb force and the van der Waals force, whereas the interaction between pAsp and calcite mainly depended on the Coulomb force. These results helped us to probe into the assembling forces of the calcite crystals under the action of PVA and pAsp at the molecular level.

Table 3. Non-bonding energies between calcite and the polymers

Surface	Polymer	$\Delta E_{non\text{-}bond}$ (kJ·mol^{-1})	ΔE_{vdW} (kJ·mol^{-1})	$\Delta E_{coulomb}$ (kJ·mol^{-1})
(001)	PVA	−45274.13	−19145.10	−26129.02
(104)	pAsp-low	−597514.04	17702.48	−615219.03
(104)	pAsp-high	−557387.56	4398.45	−561786.02

It is important to understand the effects of incorporated inorganic particles on the mobility of the polymer in order to characterize the manner in which inorganic particles reinforce or plasticize the polymer and alter the transport properties of the hybrid system. The diffusion channels between free-volume voids are controlled by the polymer with chain mobility. Understanding chain mobility is crucial for studying the transport properties of hybrid systems.[50,51] It is generally agreed that polymer chain mobility is closely related to the interaction between inorganic particles and the polymer.[52,53]

Polymer chain mobility is investigated by examining the mean-square displacement (MSD) of the polymer chains as a function of the simulation time:

$$\langle \Delta r(t)^2 \rangle = [(r_i(t) - r_i(0))^2], \quad (3)$$

where $r_i(t)$ and $r_i(0)$ are the positions of atom i at time t and 0, respectively. The bracket denotes the ensemble average, which is obtained by averaging over all atoms and all time origins, $t = 0$. Inorganic particles may serve as a crosslink that constrains the surrounding polymer chains, thereby decreasing the polymer chain mobility.[54] Meanwhile, the inorganic particles may perturb the polymer chain packing and consequently destroy the crystalline region in the polymer.[55] Therefore, the changes in chain mobility depend on the organic-inorganic systems.[56,57] In the present system, PVA and pAsp are semi-crystalline polymers in which the mobility of the polymer chains is constrained by the crystalline regions, as a result of which they exhibit slow domains. When the calcite crystals are incorporated into the polymer, chain packing perturbation plays a dominant role. There are strong interactions between calcite and the polymer, and these interactions disrupt the percolation of slow domains that would normally be present in the polymer. Thus, the chain mobility increases as a greater number of crystalline regions lose their percolated nature.

The MSD of the polymer chains in the calcite/PVA and calcite/pAsp models is shown in Figure 5. A larger slope of the MSD curve indicates a higher chain mobility.[52] Apparently, the polymer chain mobility of the two models is higher than that of a pure polymer molecule. The strong interactions between the polymer and calcite, combined with the binding energy, disrupt the crystalline region in the polymer, thereby resulting in the enhancement of chain mobility. It is interesting to note that the calcite crystals grew under the action of PVA and pAsp, the property of PVA and pAsp were affected by calcite crystal simultaneously. Furthermore, the calcite/pAsp-high model which made the

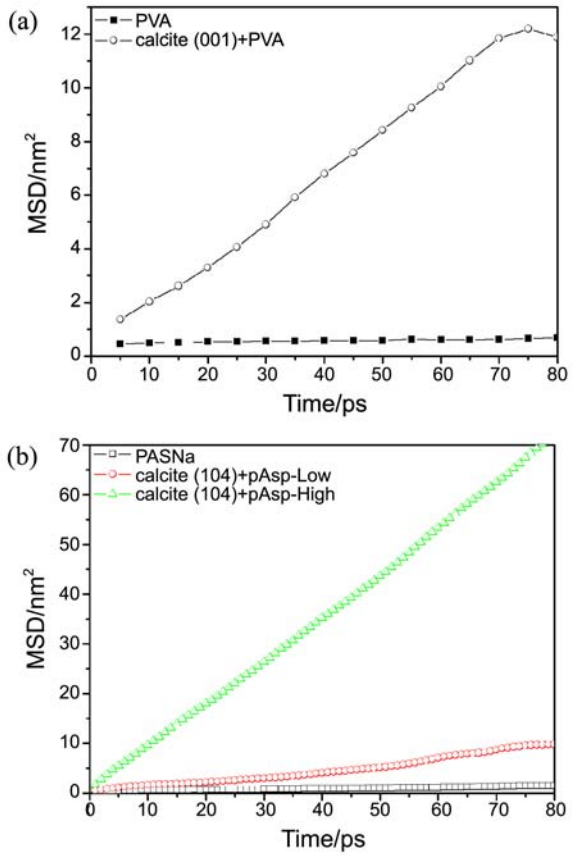

Figure 5. MSD of the polymer chains in (A) the calcite/PVA model and (B) the calcite/pAsp model.

two PASP molecules homogeneous distribution in the model have lager slope compare calcite/pAsp-low model. Therefore, combine with the calculations of binding energy, the strong interaction between polymers and calcite surfaces disrupted the polymers crystalline region, resulting in the enhancement of chain mobility.

Conclusion

We successfully constructed an artificial biomineralization system, where calcite was mineralized within the PVA/pAsp polymer matrix. The design of this *in vitro* crystal growth system was based on the models of the organic matrix in which biomineralization occurs.[2] We have shown that the calcite crystals nucleate in the inductive region of the PVA membranes through interfacial matching to the (001) faces. By simply varying the concentration of pAsp added to calcite, the calcite crystal was assembled to form flower-like and pineapple-like particles. Further, pAsp was adsorbed on the surface of the calcite crystals for inducing the aggregation of the crystals through coordinated interactions between the COO^- groups of pAsp and the Ca^{2+} ions of the calcite crystals. We also carried out MD simulations in order to obtain a better understanding of the interactions between the polymers and the crystal at the molecular level. The MD results indicate that the interaction between PVA and calcite mainly depends on the Coulomb force and the van der Waals force, whereas the interaction between pAsp and calcite mainly depends on the Coulomb force. Moreover, we found that as a result of the interaction between the polymers and calcite, the polymer chain mobility of the composite was higher than that of the pure polymer. The results of this study demonstrate the effectiveness of the proposed approach, which allows superior control over the crystal morphology and membrane architecture and the potential of biomimetic mineralization as a promising strategy toward the advancement of materials. Improved understanding of the formation of highly ordered structures under biomimetic conditions would enable further advancements in chemical, biological, and materials sciences and help develop effective methods to encapsulate and deliver various target substances in biological and pharmaceutical applications. Controlling the crystalline assembly by changing the concentration of the crystal modifier provides an ideal bottom-up approach to fabricate new functional materials and devices with desirable organization.

Acknowledgments. This work was supported by the BioScientific Research Grant funded by the Pusan National University (PNU, Bio-Scientific Research Grant) (PNU-2008-101-20080608000), and also by the National Fisheries Research & Development Institute (Grant number: 20100434961-00).

References

1. An, X.; Cao, C. *The Journal of Physical Chemistry C* **2008**, *112*, 15844-15849.
2. Li, H.; Estroff, L. A. *J. Am. Chem. Soc.* **2007**, *129*, 5480-5483.
3. Hou, W. T.; Feng, Q. L. *Crystal Growth & Design* **2006**, *6*, 1086-1090.
4. Mann, S.; Webb, J.; Williams, R. J. P. *Biomineralization: Chemical and Biochemical Perspectives*; John Wiley & Sons: 1989.
5. Sommerdijk, N. A. J. M.; With, G. *Chemical Reviews* **2008**, *108*, 4499-4550.
6. Arias, J. L.; Fernandez, M. S. *Chemical Reviews* **2008**, *108*, 4475-4482.
7. Qiao, L.; Feng, Q.; Lu, S. *Crystal Growth and Design* **2008**, *8*, 1509-1514.
8. Naka, K.; Chujo, Y. *Chemistry of Materials* **2001**, *13*, 3245-3259.
9. Lowenstam, H. A.; Weiner, S. *On Biomineralization*; Oxford University Press: USA, 1989.
10. Mann, S. *Biomineralization: Principles and Concepts in Bioinorganic Materials Chemistry*; Oxford University Press: USA, 2001.
11. Baeuerlein, E. *Biomineralization: Progress in Biology, Molecular Biology and Application*; Vch Verlagsgesellschaft Mbh: 2004.
12. Yu, S. H. *Biomineralization II* **2007**, 79-118.
13. Yang, H.; Yao, W.; Yang, L.; Ma, X.; Wang, H.; Ye, F.; Wong, K. *Journal of Crystal Growth* **2009**, *311*, 2682-2688.
14. Dzakula, B.; Brecevic; Falini, G.; Kralj, D. *Crystal Growth and Design* **2009**, *9*, 2425-2434.
15. Kotachi, A.; Miura, T.; Imai, H. *Crystal Growth & Design* **2006**, *6*, 1636-1641.
16. Ajikumar, P. K.; Lakshminarayanan, R.; Valiyaveettil, S. *Crystal Growth & Design* **2004**, *4*, 331-335.
17. Naka, K. *Biomineralization II* **2007**, 119-154.
18. Naka, K.; Huang, S. C.; Chujo, Y. *Langmuir* **2006**, *22*, 7760-7767.
19. An, X.; Cao, C. *The Journal of Physical Chemistry C* **2008**, *16*,

6526-6530.
20. Balz, M.; Barriau, E.; Istratov, V.; Frey, H.; Tremel, W. *Langmuir* **2005**, *21*, 3987-3991.
21. Jin, F. L.; Park, S. J. *Bull. Korean Chem. Soc.* **2009**, *30*, 335.
22. Cheng, C.; Shao, Z.; Vollrath, F. *Advanced Functional Materials* **2008**, *18*, 2172-2179.
23. Schuth, F. *Chemistry of Materials* **2001**, *13*, 3184-3195.
24. Li, W.; Wu, P. *CrystEngComm.* **2009**, *11*, 2466-2474.
25. Wang, T.; Leng, B.; Che, R.; Shao, Z. *Langmuir* **2010**, *16*, 13385-133892.
26. Gebauer, D.; Colfen, H.; Verch, A.; Antonietti, M. *Advanced Materials* **2009**, *21*, 435-439.
27. Gebauer, D.; Volkel, A.; Colfen, H. *Science* **2008**, *322*, 1819-1822.
28. Yu, S. H.; Colfen, H.; Hartmann, J.; Antonietti, M. *Advanced Functional Materials* **2002**, *12*, 541-545.
29. Colfen, H.; Antonietti, M. *Langmuir* **1998**, *14*, 582-589.
30. Colfen, H.; Qi, L. *Chem. Eur. J.* **2001**, *7*, 106-116.
31. Sun, H. *J. Phys. Chem. B* **1998**, *102*, 7338-7364.
32. Pokroy, B.; Kapon, M.; Marin, F.; Adir, N.; Zolotoyabko, E. *Proceedings of the National Academy of Sciences* **2007**, *104*, 7337-7341.
33. Feng, Q. L.; Li, H. B.; Pu, G.; Zhang, D. M.; Cui, F. Z.; Li, H. D.; Kim, T. N. *Journal of Materials Science* **2000**, *35*, 3337-3340.
34. Albeck, S.; Aizenberg, J.; Addadi, L.; Weiner, S. *Journal of the American Chemical Society* **1993**, *115*, 11691-11697.
35. Aizenberg, J.; Black, A. J.; Whitesides, G. M. *Journal of the American Chemical Society* **1999**, *121*, 4500-4509.
36. Cullity, B. D.; Stock, S. R. *Elements of X-ray Diffraction*, Prentice Hall Upper Saddle River, NJ: 2001.
37. Mann, S. *Nature* **1988**, *332*, 119-124.
38. Gower, L. A.; Tirrell, D. A. *Journal of Crystal Growth* **1998**, *191*, 153-160.
39. Falini, G. *International Journal of Inorganic Materials* **2000**, *2*, 455-461.
40. Hou, W. T.; Feng, Q. L. *Journal of Crystal Growth* **2003**, *258*, 402-408.
41. Zaremba, C. M.; Belcher, A. M.; Fritz, M.; Li, Y.; Mann, S.; Hansma, P. K.; Morse, D. E.; Speck, J. S.; Stucky, G. D. *Chem. Mater* **1996**, *8*, 679-690.
42. Yuan, P. Q.; Kong, N.; Cheng, Z. M.; Semiat, R. *Desalination* **2009**, *238*, 246-256.
43. Teng, H. H.; Dove, P. M.; De Yoreo, J. J. *Geochimica et Cosmochimica Acta* **2000**, *64*, 2255-2266.
44. Addadi, L.; Moradian, J.; Shay, E.; Maroudas, N. G.; Weiner, S. *Proceedings of the National Academy of Sciences of the United States of America* **1987**, *84*, 2732-2376.
45. Gotliv, B. A.; Addadi, L.; Weiner, S. *ChemBioChem*. **2003**, *4*, 522-529.
46. Gotliv, B. A.; Kessler, N.; Sumerel, J. L.; Morse, D. E.; Tuross, N.; Addadi, L.; Weiner, S. *ChemBioChem.* **2005**, *6*, 304-314.
47. Hernandez-Hernandez, A.; Rodriguez-Navarro, A. B.; Gomez-Morales, J.; Jimenez-Lopez, C.; Nys, Y.; Garcia-Ruiz, J. M. *Crystal Growth and Design* **2008**, *8*, 1495-1502.
48. Bhowmik, R.; Katti, K. S.; Katti, D. *Polymer* **2007**, *48*, 664-674.
49. Rybolt, T. R.; Wells, C. E.; Sisson, C. R.; Black, C. B.; Ziegler, K. A. *Journal of Colloid and Interface Science* **2007**, *314*, 434-445.
50. Tamai, Y.; Tanaka, H.; Nakanishi, K. *Macromolecules* **1994**, *27*, 4498-4508.
51. Nagel, C.; Schmidtke, E.; Gunther-Schade, K.; Hofmann, D.; Fritsch, D.; Strunskus, T.; Faupel, F. *Macromolecules* **2000**, *33*, 2242-2248.
52. Pan, F.; Peng, F.; Jiang, Z. *Chemical Engineering Science* **2007**, *62*, 703-710.
53. Fragiadakis, D.; Pissis, P.; Bokobza, L. *Polymer* **2005**, *46*, 6001-6008.
54. Moore, T. T.; Mahajan, R.; Vu, D. Q.; Koros, W. J. *AIChE Journal* **2004**, *50*, 311-321.
55. Peng, F.; Lu, L.; Hu, C.; Wu, H.; Jiang, Z. *Journal of Membrane Science* **2005**, *259*, 65-73.
56. Chen, K. H.; Yang, S. M. *Journal of Applied Polymer Science* **2002**, *86*, 414-421.
57. Dlubek, G.; De, U.; Pionteck, J.; Arutyunov, N. Y.; Edelmann, M.; Krause Rehberg, R. *Macromolecular Chemistry and Physics* **2005**, *206*, 827-840.